Synchrotron-radiation measurements of forbidden reflections in silicon and germanium

D. Mills and B. W. Batterman
School of Applied and Engineering Physics, Cornell University, Ithaca, New York 14853
(Received 27 February 1980)

The (442) and (622) reflections in both Si and Ge were measured using synchrotron radiation from the Wilson 12-GeV Synchrotron. These reflections, which are basis forbidden in diamond-structure materials, arise from two distinct effects: antisymmetric charge buildup due to covalent bonding of the valence electrons and anharmonic thermal vibrations of the core electrons. Because these reflections are sensitive only to deviations from a centrosymmetric charge density, their integrated intensities are extremely small. The measured structure factors for these reflections at room temperature were $F(442) = 0.042 \pm 0.003$, $F(622) = 0.005 \pm 0.004$, and $F(442) = 0.0630 \pm 0.0016$, $F(622) = 0.0558 \pm 0.0023$ in silicon and germanium, respectively. The anharmonic contribution can be removed from these values leaving the scattering amplitude due solely to the bond change. We compare these values to empirical and theoretical predictions. New techniques utilizing the inherent properties of synchrotron radiation will also be discussed.

INTRODUCTION

Basis forbidden reflections in diamond-structure materials, reflections whose Miller indices sum to $4n \pm 2$ (n is an integer), were first observed with x rays over 50 years ago by Bragg.[1] He detected a weak scattered intensity in diamond from the lowest-order forbidden reflection, the (222), and postulated that the observed intensity was the result of incomplete destructive interference of the scattered x rays due to the nonsphericity of the diamond's covalent bonds. The origin of this incomplete interference can easily be understood from examination of the unit cell. The diamond structure is an fcc Bravais lattice with a two-atom basis. This can be viewed as two interpenetrating fcc lattices displaced $\frac{1}{4}$ the way along the body diagonal. (See Fig. 1). Let the two basis sites (or the atoms of the two interpenetrating fcc lattices) be denoted A and B. These sites, each of which has tetrahedral symmetry, are not identical but are related by an inversion operation, i.e., $\rho_A(\vec{r}) = -\rho_B(-\vec{r})$ [where $\rho_n(\vec{r})$ is the electron density of atom n]. Now consider the distortion due to covalent bonding of a spherically symmetric free atom when placed at one of these sites. Since the local site symmetry is tetrahedral, bonding effects will produce an antisymmetric component in the atomic charge density.

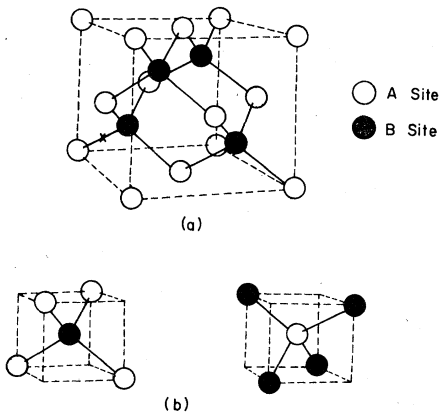

FIG. 1. The unit cell of the diamond structure (a) with eight atoms per unit cell. (b) The atoms at the B sites are not identical to atoms on the A sites but are related by inversion symmetry.

For basis forbidden reflections ($h+k+l = 4n \pm 2$), the structure factor can be written in terms of the atoms on sites A and B as

$$F(hkl) = 4[f_A(\vec{k}) - f_B(\vec{k})] \quad (h+k+l = 4n \pm 2), \qquad (1)$$

where $f_n(\vec{k})$ is the Fourier transform of the electron charge density of the atom located on the nth site. Equation (1) shows that if the charge density were centrosymmetric, viz., $\rho^c(\vec{r}) = \rho^c(-\vec{r})$, the structure factor $F(hkl)$ would truly vanish. However, if there exists an antisymmetric component to the charge density, $\rho^a(\vec{r}) = -\rho^a(-\vec{r})$, the structure factor will be[2]

$$F(hkl) = 8f^a(\vec{k}) \quad (h+k+l = 4n \pm 2). \qquad (2)$$

We have defined $f^a(\vec{k})$ as the Fourier transform of the antisymmetric charge component and set

$$f^a(\vec{k}) \equiv f^a_A(\vec{k}) = -f^a_B(\vec{k}). \qquad (3)$$

As Bragg first implied, Eq. (2) indicates that the $(4n \pm 2)$-type reflections will have no contribution from the centrosymmetric component of the atomic charge density but only from antisymmetric deviations from sphericity. This conclusion has been verified experimentally by detection of the (222) forbidden reflections in diamond,[3] silicon,[4-12] germanium,[5,13,14] grey tin,[15] and the (442) reflection in silicon.[16]

The arguments used to determine the x-ray

structure factor for the basis forbidden reflections can be extended to include neutron scattering if the electronic charge density is replaced with the appropriate distribution of nuclear scattering matter. Dawson and Willis[17] suggested that the tetrahedral symmetry of the nuclear potential well in the diamond structure should produce anharmonic thermal vibrations of the nuclei, and that this anharmonicity should give rise to a weak neutron Bragg reflection at the normally basis-forbidden reciprocal-lattice points. Subsequent measurements have revealed weak reflections[18,19] from the (222) in both Si and Ge. More recently, the Si (442) and (622) neutron reflections have been measured, but only at elevated temperatures where the anharmonic vibrational amplitudes are larger.[20]

Assuming that the core electrons follow the nuclear excursions from equilibrium (rigid-ion model), the resulting thermally smeared electronic charge distribution will have a tetrahedral character and hence both antisymmetric and centrosymmetric components. Thus, the antisymmetric scattering amplitude due to anharmonic thermal vibrations of the core electrons will also contribute to the x-ray intensity of the forbidden reflections and must be included in the structure factor.

From the available free volume in the unit cell (see Fig. 1) one would intuitively expect that the nucleus preferentially vibrates away from its nearest neighbors. This would cause a charge buildup opposite to that from the bonding electrons. The two effects thus work against one another and tend to make total charge density more centrosymmetric. Consequently, we expect the two effects to be the opposite sign, i.e.,

$$|F(hkl)| = 8\,|f^a_{\text{bond}}(\vec{k}) - f^a_{\text{anh}}(\vec{k})| \,. \tag{4}$$

Trucano[16] has verified this supposition by experimentally measuring the temperature dependence of the (442) x-ray reflection in silicon. As the crystal was heated, the (442) integrated intensity first decreased, went through zero, and then increased, indicating that at low temperatures scattering from the bond charge dominated the measured intensity. As the temperature was increased, the anharmonic vibrations and hence anharmonic scattering amplitude increased, eventually equaling the valence scattering amplitude resulting in a vanishing of the reflected intensity. Additional heating further increased the magnitude of the anharmonic term causing the Bragg intensity to then increase with temperature, confirming the choice of sign between the two terms.

Clearly, the measurement of these forbidden reflections provides information on both valence charge densities and anharmonic thermal vibrations. Combining neutron and x-ray measurements allows the anharmonic vibrational component of the scattering amplitude to be removed from x-ray measurements. This allows information on the shape and magnitude of the bond charge distribution to be extracted without interference from scattering from the spherical core which is automatically canceled due to its centrosymmetric character. The sensitivity of these reflections to the valence bond charge provides an accurate experimental check on valence-electron charge distributions calculated from theoretical wave functions using the various band-structure computational techniques.

The integrated intensity of basis forbidden reflections is quite small. For the Si (442), the integrated intensity is about 6 orders-of-magnitude less than that of a low-order allowed reflection. Consequently, the detection of such reflections is extremely difficult even with high-flux x-ray tubes and the most sophisticated detection systems.

In this paper we report the measurements of the higher-order forbidden reflections (442) and (622) in silicon and germanium using synchrotron radiation from the Wilson 12-GeV Synchrotron. The inherent properties of synchrotron radiation sources, i.e., large source-sample distance, degree of both horizontal and vertical collimation attainable without excessive loss of flux, and the continuous nature of the spectrum seemed particularly suited to measure these extremely weak Bragg reflections.

The combination of these synchrotron radiation experiments and previously measured neutron scattering results have allowed us to compare the measured bond charge scattering amplitudes with various theoretical models. In the case of silicon we found good agreement with the antisymmetric scattering amplitude predicted by the deformation density analysis of Price, Maslen, and Mair.[21] Our germanium results indicate that, even at room temperature, the anharmonic term in the structure factor dominates the bonding term in the higher-order forbidden reflections. The valence-electron contributions to the structure factor are therefore more difficult to extract than in the silicon measurements. The germanium results will be compared with the deformation density analysis of allowed reflections by Dawson.[22]

APPARATUS

The experiments described in this paper were performed at the Wilson 12-GeV Synchrotron. A 150-MeV LINAC injects 10^9 to 10^{10} electrons into the synchrotron at 60 Hz where they are accel-

erated to a maximum energy of 12 GeV in $\frac{1}{120}$ of a second. With an average magnetic bend radius of ~100 m, the critical energy of the synchrotron radiation spectrum at the maximum electron energy of 12 GeV is 38 KeV. The origin of the emitted synchrotron radiation was ~30 m from the experimental area. A 10-mil Be window separated the machine vacuum from the vacuum in the beampipe which traversed the 23 m from the window to the spectrometer. A set of vertical and horizontal slits were located 13 m from the source. In a typical experiment about $\frac{1}{3}$ mrad of orbital radiation was incident upon the specimen.

Integrated intensity measurements of the forbidden reflections were made on a two-crystal spectrometer (see Fig. 2). The first crystal is the monochromator and the second is the sample. The selection of a proper monochromating crystal was extremely important. A perfect (620) Si crystal was chosen, because its d spacing closely matched those of the reflections we wished to study. The second-order reflection, the (12 4 0), is allowed and, as we will show below, can be used to advantage. A good matching of d spacing between the first and second crystals decreases the dispersion of the system, resulting in sharper reflection curves and hence a better overall signal-to-noise ratio.

With the continuous spectrum source, a monochromator whose second-order reflection is allowed facilitates the initial location of the forbidden reflection by detecting its allowed first harmonic. [The second-order reflection from a $(4n \pm 2)$-type reflection is always allowed, since the Miller indices sum to $4m$, $m = 2n \pm 1$.]

To take advantage of the large component of radiation polarized in the plane of the electron's orbit, the beam was reflected in the vertical plane. A Siemens diffractometer mounted vertically provided a coarse θ motion for the second crystal plus a θ–2θ motion for wavelength determination. A tangent arm spectrometer was mounted coaxially on the Siemens to provide a fine θ motion. Initially a step-motor was coupled through a reducer to a micrometer to drive the tangent arm. The large impulse imparted to the system with each motor step caused the entire spectrometer to ring and vibrate. Narrow rocking curves could not be measured in a reproducible manner. We overcame this difficulty by driving the tangent arm directly with a piezoelectric crystal. Although the piezocrystal provided a limited angular range, it was well suited for this work, because most of the rocking curves were quite narrow—the order of several seconds of arc obtainable with synchrotron radiation.

Since access to the experimental area was forbidden with the beam on, all spectrometer motions had to be remotely controllable. These include both crystal angular drives as well as x-y translations of the second crystal. A DEC PDP 8/a minicomputer controlled all motions through stepping motor drives.

In general, all crystals of germanium and silicon were prepared from reasonably perfect, low-dislocation crystals. Crystal faces were cut parallel to the diffracting planes and were mechanically polished, etched with CP-4 and, finally, polished with syton[23] to a mirror-like finish. The crystals were checked for perfection by measuring rocking

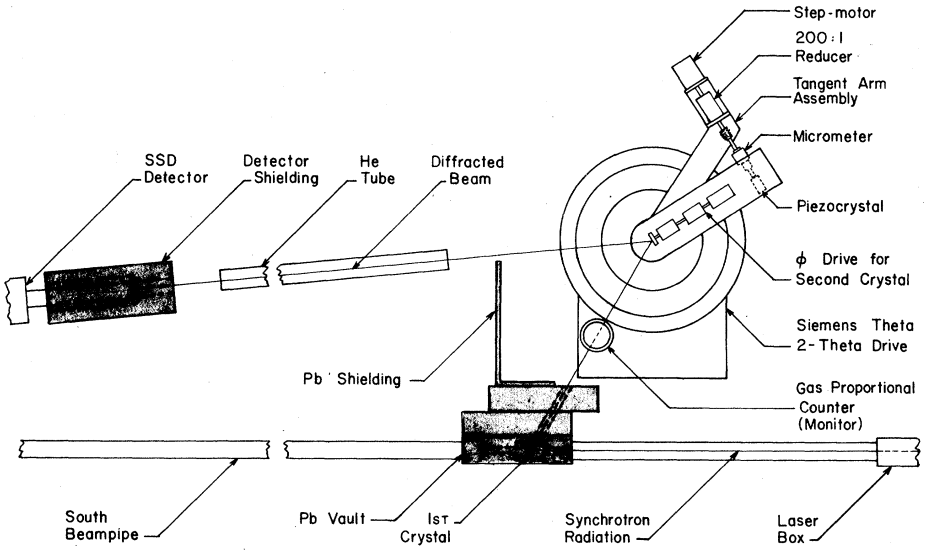

FIG. 2. Schematic diagram of experimental setup used to measure the forbidden reflections.

curves before and after syton polishing and were compared to the perfect-crystal theory. Although a mirror finish was not necessary for this work, it conveniently allowed us to use a laser beam to make preliminary alignment of the crystals and detection systems. The synchrotron radiation diffracted from the first crystal was monitored by a transmission gas proportional counter shown in Fig. 2. The synchrotron beam was very unstable and fluctuated quite strongly on a time scale of seconds. The proportional counter contained a gas fill which absorbed only a few percent of the incident photons. This allowed the detector to be used in a single photon-counting mode, and most data were taken for a fixed number of these monitor counts. Although a transmission ion chamber would have been useful, the once-monochromated beam in our setup would produce a current of only a few tens of picoamps, which we felt was too small to measure with reasonable precision.

TECHNIQUE

One of the major difficulties in measuring weak reflections of the type described above is the appearance of multiple reflections. Multiple reflections arise whenever the Ewald sphere is cut by two or more reciprocal-lattice points simultaneously. This condition is displayed schematically in Fig. 3, where the relation between the reciprocal-lattice vectors is $\vec{H}=\vec{H}'+\vec{H}''$ ($\vec{H}$, $\vec{H}'$, and $\vec{H}''$ are the reciprocal-lattice vectors of primary and two auxiliary reflections, respectively.) The vector $\vec{S}$ in the figure is in the direction of the diffracted beam from the *hkl* reflection.

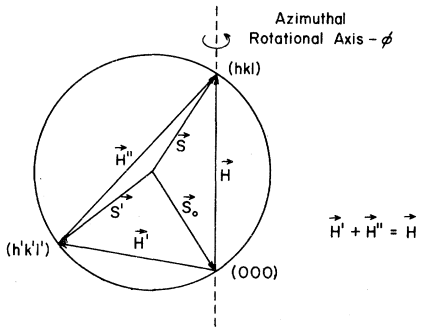

FIG. 3. Geometrical condition for multiple diffraction. The diffracted beam from the planes associated with the reciprocal-lattice vector $\vec{H}'$ can act as the incident beam for another set of planes within the crystal ($\vec{H}''$). This causes a beam to be directed along $\vec{S}$, which is identical in direction to the diffracted beam from the planes of interest (corresponding to the reciprocal-lattice vector $\vec{H}$). Rotation of the crystal azimuthally can maintain the diffraction relationship for $\vec{H}$, but eliminate the multiple reflection conditions by moving $\vec{H}'$ off the sphere of reflection.

However, as can be seen from the figure, it is possible for a second reflection $h'k'l'$ to lie on the Ewald sphere and cause an internal diffracted beam labeled $\vec{S}'$. This now acts as a new incident beam and diffracts from the reciprocal-lattice vector $\vec{H}''$ producing another beam in the original direction of $\vec{S}$. In this way the multiple reflection can cause spurious increases or decreases in the intensity of the sought-after *hkl* reflection. Figure 4 shows a computer plot of the locus of all possible multiple reflections as a function of wavelength and azimuthal angle for the (442) reflection in silicon and germanium. The possible multiple reflections, as a function of azimuth, are determined by the intersection of a horizontal line in the figure (corresponding to a given wavelength) with any of the plotted curves. The number of multiple-reflection possibilities increases enormously as the wavelength decreases. This is because the Ewald sphere becomes larger, and the probability of it intersecting other reciprocal-lattice points increases as the volume of the sphere increases. Since the synchrotron radiation is tunable and narrowly collimated, one can pick a multiple reflection-free region quite accurately within the complex pattern shown in Fig. 4. The wavelengths used were picked to optimize several competing parameters. Shorter wavelengths have the disadvantage of increasing the number of multiple reflections, while longer wavelengths result in strong absorption in the sample windows and in the air paths. For silicon, we selected a wavelength of 1.22 Å, allowing us to investigate the reflection-free regions labeled A, B, and C along the horizontal line corresponding to 1.22 Å. For germanium, we chose 1.46 Å, since this was not energetic enough to cause fluorescence of the germanium crystal, thereby helping to reduce the general background while still allowing transmittance in the windows and air paths.

To locate points on this multiple-reflection plot we needed to know the ϕ position and wavelength quite precisely. The wavelength determination was made using a perfect silicon (333) crystal as a second crystal in the setup. We used a scintillation counter on the 2θ arm of the Sieman spectrometer and scanned until we located the (333) reflection. We then activated the θ–2θ drives, and the crystal was stepped until the (444) reflection was found. In this way we could accurately measure the angle between these two reflections, $\Delta\theta$. From the known silicon lattice parameter, the wavelength could be determined from the following equation:

$$\lambda = 2d_{333}\sin\left[\tan^{-1}\left(\frac{\sin(\Delta\theta)}{\frac{4}{3}-\cos(\Delta\theta)}\right)\right]. \qquad (5)$$

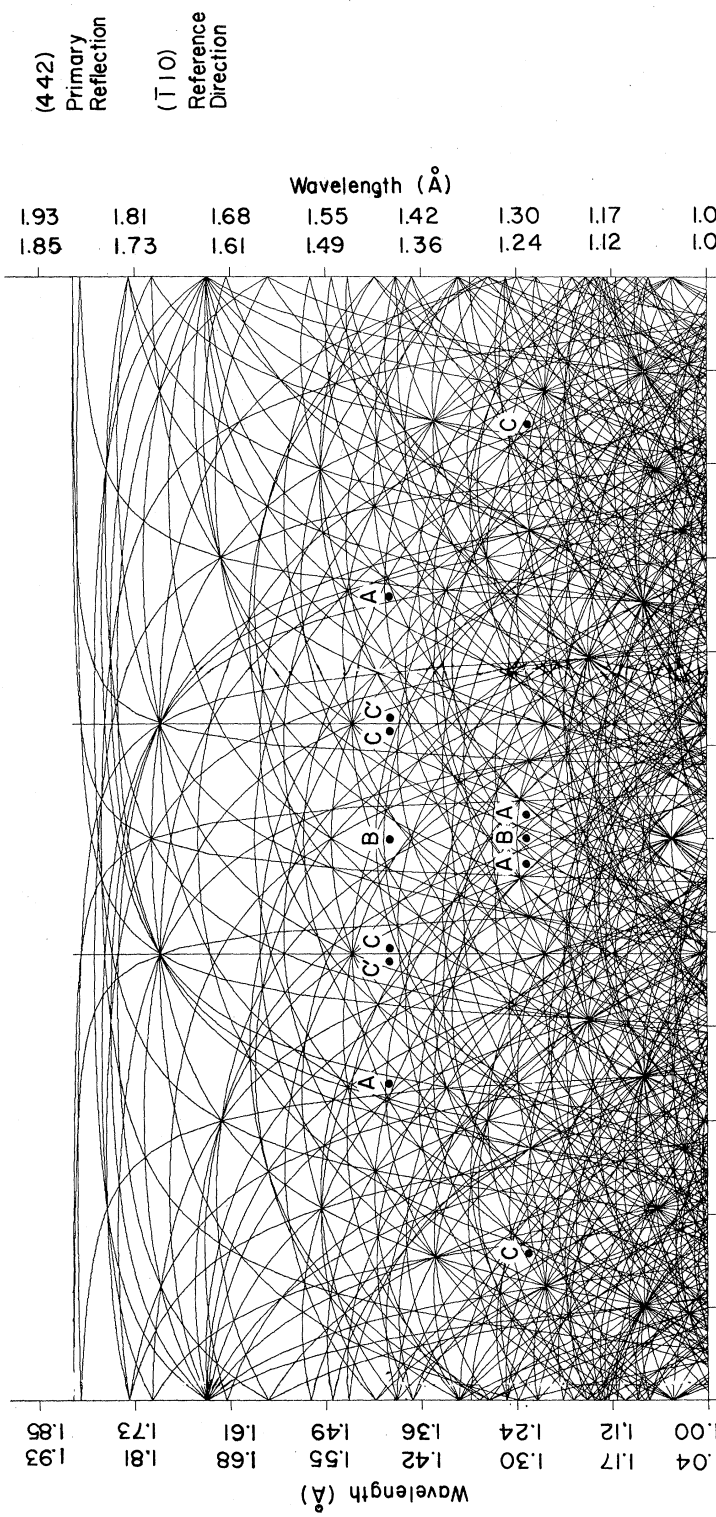

FIG. 4. Computer-generated multiple reflection plot for the (442) reflection in diamond-structure materials. Phi is measured relative to a given crystallographic direction from the plane of diffraction.

An error in $\Delta\theta$ of 0.01 degrees caused less than a $\frac{1}{10}\%$ change in the measured wavelength.

Since the forbidden reflections are extremely weak, it was important to keep the ambient background level to a minimum. We discovered that a substantial portion of the background radiation was produced during the electron injection and extraction periods of the synchrotron cycle. The emitted synchrotron radiation flux is low at both these points of the cycle. A significant improvement in the signal-to-noise ratio was realized if we gated our detectors off during these noisy periods. A circuit capable of opening and closing four switches was coupled to a gate generator with sufficient delay to allow us to gate our entire detection system at any chosen point in the syncrotron cycle.

Another important factor in the reduction of background, and hence improvement of the signal-to-noise ratio, takes advantage of the intrinsic brightness of the synchrotron source. The background radiation observed at the detector from the second crystal is composed of Compton, thermal diffuse scattering, and fluorescence. The origin point of this scattering is the second (specimen) crystal, while the origin point for the Bragg scattered x rays of the forbidden reflection is at the synchrotron tangent point, some 30 m away. Because both the background and Bragg reflected photons have a $1/R^2$ intensity dependence from their respective origins, a substantial increase in the signal-to-noise ratio can be obtained when the sample-to-detector distance is increased. A large relative change in the sample-to-detector distance will drastically reduce the background at the detector while maintaining the intensity of the Bragg reflection, since this change corresponds to only a small increment in source-to-detector distance. Our sample-to-detector distance of ~1.3 m was determined primarily by physical limitations in the experimental area. A helium-filled tube was placed between the sample and the detector to minimize air-path absorption.

As mentioned previously, the first harmonic from the monochromator crystal was extremely useful in locating forbidden reflections. Recall that the forbidden reflection itself is extremely weak and only seconds of arc in width. However, we could locate the strong $\frac{1}{2}\lambda$ reflection from the second order of the forbidden reflection quite easily. The harmonic was also valuable in recording the multiple-reflection plots. Using this harmonic, the Bragg condition could be precisely maintained as the second crystal was rotated azimuthally. A multiple-reflection plot recorded in this manner together with predicted positions is shown in Fig. 5. We were able to find all the multiple reflections predicted geometrically. The sharpness of the multiple-reflections' peaks is due primarily to the small, horizontal divergence used in the experiment, approximately $\frac{1}{3}$ mrad. This allowed us to select regions normally unusable that were free of multiple reflections. The $\frac{1}{2}\lambda$ second-order reflection, although offering the advantages cited above, produced difficulties when we ultimately were to collect data on the weak forbidden reflections. This difficulty arose because it diffracted simultaneously with the forbidden reflection. Although the solid state Si(Li) detector could easily resolve the $\frac{1}{2}\lambda$ pulses from

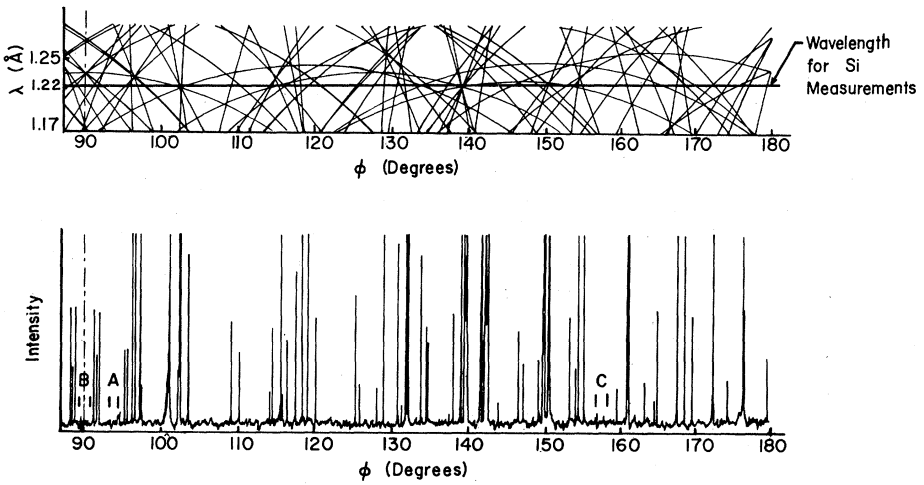

FIG. 5. (a) Enlargement of a portion of Fig. 4 showing only multiple reflections where both spurious reflections are allowed (Umweganregnungs). The line parallel to the ϕ axis marks the wavelength (1.22 Å) used for the silicon measurements. (b) Experimental Si (442) multiple-reflection plot taken with synchrotron radiation. Positions labeled *A* and *B* are where the data were collected for the Si (442) integrated intensity measurements.

the λ pulse, the long low-energy tail in the pulse distribution, due to incomplete charge collection in the detector, caused a general and varying background in the vicinity of the λ pulses. To compensate for the varying background due to the long-wavelength tail of the $\frac{1}{2}\lambda$ peak, we collected at each step in the scan the entire spectrum from the detector on a 1024-channel multichannel analyzer (MCA). For a given run through a forbidden-reflection rocking curve, the individual MCA spectra acquired at each data position through the step scan were summed to produce a single spectrum with reasonable statistics. The counts above background could then be readily obtained. After correction for diffuse and Compton scattering, the resulting integrated intensity could be extracted from the data. All integrated intensity measurements were taken in a step scan mode, each step advancing after preset number of monitor counts had been collected.

It was necessary for the ultimate calculation of the structure factors to have all the measurements on an absolute scale. We achieve this by periodically measuring the integrated intensity of a (533) allowed silicon reflection. This reflection was chosen because its d spacing is close to the other forbidden reflections and that its second-order reflection was not allowed so that harmonic contamination was not a problem. By experimentally measuring the integrated intensity of the (533) and using the calculated integrated intensity from dynamical theory, one in essence calculates the primary-beam intensity. In fact, what we obtain from this measurement is a direct correlation between the number of monitor counts and an absolute-intensity scale.

RESULTS

The measured value of the room-temperature Si (442) integrated intensity was $6.8 \pm 0.9 \times 10^{-11}$, corresponding to a structure factor of $F_{\mathrm{Si}}(442) = 0.042 \pm 0.003$. This value is in fair agreement with Trucano's value[16] of 0.035 ± 0.002 obtained with a standard x-ray tube. Our $F_{\mathrm{Si}}(442)$ is the average of eight measurements taken at two different $\Delta\phi$ regions marked A and B on the multiple-reflection plot (see Fig. 4). The values from the two azimuthal regions were the same to within experimental error, suggesting that multiple-diffraction effects were not present.

The integrated intensity of the Si (622) differed from zero barely outside our experimental uncertainty. The average of eight runs in three distinct $\Delta\phi$ regions yielded a structure factor of $F_{\mathrm{Si}}(622) = 0.005 \pm 0.004$. The near-vanishing intensity from the (622) implies that for this reflection at room temperature the anharmonic scattering and bond scattering amplitudes are nearly equal in magnitude, resulting in almost total cancellation in the structure factor. An obvious point of query is: What assurance does one have that the (622) was being measured? Comparison of the experimentally recorded multiple-reflection plot with the computer-generated graph, together with the observation of the $\frac{1}{2}\lambda$ rocking curve, virtually guarantees that the specimen was at the correct Bragg angle and the detectors properly aligned, and thus we were in fact measuring the (622).

Figure 6(a) shows the summed MCA spectrum for one of the Si (622) runs. The Bragg scattered photons from the (622) planes which have an energy that corresponds to MCA channel number 155, can barely be observed above background. The tail of the much larger $\frac{1}{2}\lambda$ pulse distribution (centered near channel number 320) can be seen on the far right. (The peak at channel number 75 is due to electronic noise).

In contrast to this we show in Fig. 6(b) a typical summed MCA spectrum from one of the more intense forbidden reflections, the Ge (442). The vertical scales are approximately equal in both plots. The horizontal scales, however, are not the same due to different amplifier gains used in the two runs. In this plot the peak from the Bragg reflected photons is centered in channel number 150. The large peak near 180 is the characteristic $K\alpha$ germanium lines from the sample which is fluoresced by the first harmonic. Again, the increase in background at higher channel number is due to the tails of the $\frac{1}{2}\lambda$ pulse distribution.

The measured Ge (442) structure factor averaged over ten runs from two different azimuthal positions (labeled B and C in Fig. 4) was $F_{\mathrm{Ge}}(442) = 0.063 \pm 0.002$. The average integrated intensity for the Ge (622) measured in five distinct $\Delta\phi$ regions was $4.0 \pm 0.3 \times 10^{-11}$, corresponding to a structure factor $F_{\mathrm{Ge}}(622) = 0.056 \pm 0.002$.

Using independent neutron scattering data, the component due to anharmonic thermal vibrations of the core electrons, can be extracted leaving the scattering amplitude due solely to the bonding electrons. A more detailed calculation of the structure factor[24] reveals that Eq. (4) can be rewritten as

$$|F(hkl)|_{\text{x ray}} = 8\left|f^{a}_{\text{bond}}(\vec{k})e^{-M_b} - f_{\text{core}}(\vec{k})e^{-M_c}A(hkl;T)\right| , \tag{6}$$

where M_b (M_c) is the Debye-Waller factor for the bonding (core) electrons, $f^{a}_{\text{bond}}(\vec{k})$ [$f_{\text{core}}(\vec{k})$] is the scattering amplitude of the bonding (core) electrons, and $A(hkl;T)$ is the anharmonic vibrational factor. The neutron structure factor for these reflections is given by

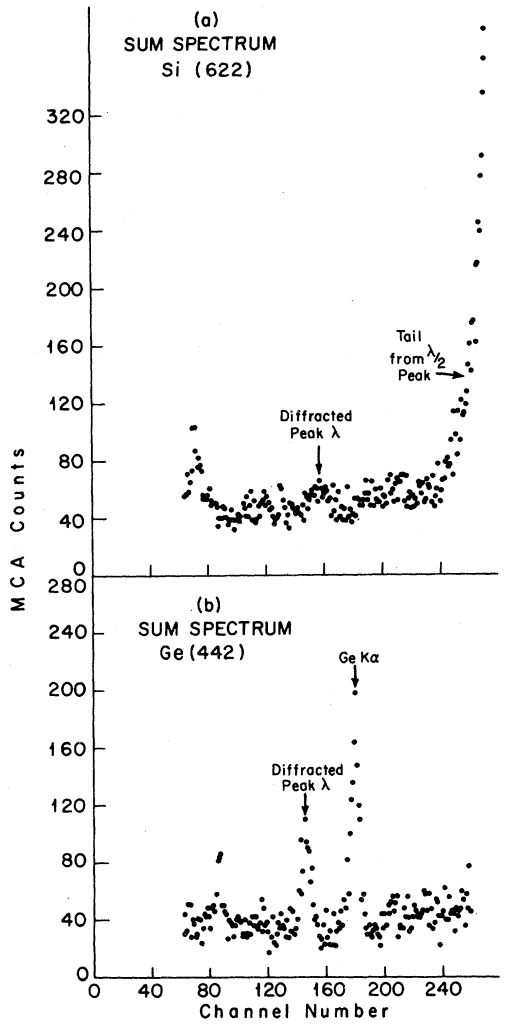

FIG. 6. Summed MCA spectrum from (a) one of the Si (622) runs and (b) one from the more intense Ge (442) runs. The diffracted photons from the (622) planes in silicon have an energy corresponding to channel number 155 in the MCA and can barely be seen above the background. The tail from the much larger $\frac{1}{2}\lambda$ pulse distribution (centered off-scale in this plot at channel 320) is evident on the right-hand side of the plot. A peak due to electronic noise can also be seen centered near channel 75. The Bragg scattered photons from the Ge (442) are readily observable in the peak centered near channel 150 in (b). The larger peak at higher energy (channel 180) is due to the characteristic Ge $K\alpha$ radiation that is fluoresced by the first harmonic. Vertical scales have been adjusted to be equivalent to show the relative sizes of the two diffracted beam intensities. The horizontal scales are not equivalent due to a change in the amplifier gain made between the two runs.

$$|F(hkl)|_{\text{neutron}} = 8be^{-M_c}A(hkl;T)\,, \tag{7}$$

where b is the neutron scattering length. For tetrahedral site symmetry the lowest-order anharmonic factor in $A(hkl;T)$ is proportional to the product of the Miller indices hkl. We can therefore scale the (222) neutron data to obtain the relevant (442) and (622) x-ray anharmonic components. In this fashion one gets

$$A_{\text{Si}}(442;296°) = (9.32 \pm 0.93) \times 10^{-4}\,,$$

$$A_{\text{Si}}(622;296°) = (6.99 \pm 0.70) \times 10^{-4}\,,$$

$$A_{\text{Ge}}(422;296°) = (7.99 \pm 1.16) \times 10^{-4}\,,$$

and

$$A_{\text{Ge}}(622;296°) = (5.99 \pm 0.87) \times 10^{-4}\,,$$

using the neutron data of Roberto *et al.*[25] and neutron scattering lengths of 0.415×10^{-12} cm and 0.819×10^{-12} cm (Ref. 26) for Si and Ge, respectively. (The Si neutron data were taken at 288 K. When adjusted to 296 K for this experiment, a 6% correction was necessary.) Solving Eq. (6) explicitly for the bond charge scattering amplitude, we get

$$f^a_{\text{bond}}(\vec{k})e^{-M_b} = \left| \pm\tfrac{1}{8}|F(hkl)| + f_{\text{core}}(\vec{k})e^{-M_c}A(hkl;T) \right| . \tag{8}$$

The plus sign corresponds to the case where the bond scattering amplitude is larger than the anharmonic term, the minus sign the reverse. Table I summarizes the calculated values of $f_b e^{-M_b}$ derived from the $F(hkl)$'s measured in this work.

Predictions of the valence bond scattering amplitudes of semiconductors, particularly silicon and germanium, have been made by many authors using many different methods. The techniques range from *ab initio* band-structure-type calculations to empirical predictions extracted from precise measurements of allowed reflections (deformation density calculations). A detailed description of all the methods is too lengthy to include here. We summarize these results in an attempt to clarify the ambiguity between the relative magnitude of the valence and anharmonic terms. Most predictions do not include the temperature dependence (e^{-M_b}) in the reported values. Consequently, we will scale our data by e^{M_b}, taking M_b to be equal to the Debye-Waller factor for the core, i.e., $M_b = M_c$. (The value of the Debye-Waller factor for the bonding electrons is somewhat disputed but is generally agreed to lie within the range $0.5M_c < M_b < M_c$.[24] For the reflections measured in this work the difference between $0.5M_c$ and M_c barely affects our calculations outside experimental error, and we therefore set $M_b = M_c$.) Tables II and III summarize the results for silicon and germanium. The (222) results, although not measured in this study, are listed for completeness.

TABLE I. Summary of the forbidden reflections measured in this work. Column 2 contains the experimentally determined integrated intensities and column 3 the corresponding structure factors for each of the measured reflections. In column 4 is the anharmonic component of the x-ray structure factor calculated by scaling neutron forbidden reflection data. The last columns contain the scattering amplitudes of antisymmetric component of the bond charge.

(hkl)	Integrated intensity ($\times 10^{11}$)	$\lvert F(hkl)\rvert$	$8f_c e^{-M} A(hkl;T)$	$f^a_{\text{bond}}(k)$ [a]	$f^a_{\text{bond}}(k)$ [b]
Si (442)	6.8 ±0.9	0.042 ±0.003	0.039±0.004	0.0116±0.0007	
Si (622)	0.10±0.16	0.005 ±0.004	0.026±0.003	0.0047±0.0007	0.0031±0.0007
Ge (442)	4.6 ±0.2	0.0630±0.0016	0.078±0.011	0.021 ±0.001	0.002 ±0.001
Ge (622)	4.0 ±0.3	0.0558±0.0023	0.052±0.008	0.016 ±0.001	0.000 ±0.001

[a] Antisymmetric bond-charge term larger than anharmonic vibrational term.
[b] Anharmonic vibrational term larger than antisymmetric bond-charge term.

In general the best overall agreement in both Si and Ge comes from the empirical deformation density calculations.[21,22,27] The best match to the silicon data is derived from the analysis by Price, Maslen, and Mair[21] of the precise Pendellösung measurements of Aldred and Hart.[28] Although the value predicted for the Si (622) from these analyses matches more closely the experimentally determined value when the anharmonic term is taken to be larger than the valence term, the ambiguity over the relative sizes cannot be conclusively resolved.

Calculated values for germanium tend to agree more closely with the experimental values obtained assuming the anharmonic term is larger than the valence term. This picture is certainly reconcilable on physical grounds, since germanium has a greater number of core electrons and lower Debye temperature than silicon ($\theta_{\text{Ge}}=296$ K, $\theta_{\text{Si}}=540$ K), making the effect of the anharmonically vibrating core electrons more pronounced in germanium than silicon. Furthermore, as one proceeds down the fourth column of the Periodic Table, the trend is for the bonds to be less directed and more diffuse going from diamond, an insulator, through the semiconducting materials, silicon and germanium, into the metals (grey tin).

SUMMARY AND CONCLUSIONS

We have successfully found and measured the extremely weak (442) and (622) forbidden reflec-

TABLE II. Comparison of measured antisymmetric bond-charge scattering amplitudes for Si to those predicted empirically and theoretically. The second and third columns show the values of the antisymmetric scattering amplitudes previously measured (column 2) and measured in this work (column 3). These are compared to values obtained using a deformation density analysis of allowed reflections (labeled Dawson and Price *et al.*) and those from a perturbative-pseudopotential calculation (labeled Bertoni *et al.*).

(hkl)	$f^a_{\text{bond}}(k)$ Previously measured	$f^a_{\text{bond}}(k)$ This work	Dawson [g]	Price *et al.* [h]	Bertoni *et al.* [i]
222	0.190 ±0.005 [a] 0.197 ±0.002 [b] 0.193 [c]		0.189	0.185	0.188
442	0.0109±0.0008 [d]	0.0116±0.0007	0.0086	0.0099	0.0040
622		0.0047±0.0007 [e] 0.0031±0.0007 [f]	0.0027	0.0027	

[a] See Ref. 25.
[b] See Ref. 8.
[c] See Ref. 5.
[d] See Ref. 16.
[e] Assuming bond term is larger than anharmonic term.
[f] Assuming anharmonic term is larger than bond term.
[g] See Ref. 27.
[h] See Ref. 21.
[i] C. M. Bertoni, V. Bartolani, C. Calandra, and F. Nizzula, J. Phys. C 6, 3612 (1973).

TABLE III. Comparison of measured antisymmetric bond-charge scattering for Ge to those predicted empirically and theoretically. Included are the antisymmetric scattering amplitudes previously measured (column 2) and those measured in this work (column 3). Also included are the deformation density predictions of Dawson and pseudopotential calculations of Bertoni *et al.* and Duggen *et al.*

(*hkl*)	$f^a_{\text{bond}}(k)$ Previously measured	$f^a_{\text{bond}}(k)$ This work	Dawson[e]	Bertoni *et al.*[f]	Duggen *et al.*[g]
222	0.140 ± 0.006 [a] 0.137 [b]		0.142	0.215	0.096
442		0.021 ± 0.001 [c] 0.002 ± 0.001 [d]	0.0051	0.003	0.0065
622		0.016 ± 0.001 [c] 0.000 ± 0.001 [d]	0.0016		

[a] See Ref. 25.
[b] See Ref. 5.
[c] Assuming bond term is larger than anharmonic term.
[d] Assuming anharmonic term is larger than bond term.
[e] See Ref. 22.
[f] See Table II footnote i.
[g] G. Duggen, G. J. Morgan, N. Shahtahmasebi, and A. Lettington, Phys. Status Solidi B 83, 543 (1977).

tions in silicon and germanium utilizing the radiation emitted from the Wilson 12-GeV Synchrotron. The measured intensities include contributions from both anharmonic thermal vibrations of the core electrons and the antisymmetric components of the bond charge distribution. When the effect of the anharmonic core motion has been removed, the remaining portion of the scattering amplitude due to the covalent bonds can be compared with theoretical calculations based on both empirical predictions and pseudopotential calculations. There is a better overall agreement between measured and calculated bond-charge scattering amplitudes in silicon than germanium. This is partly due to the relatively large correction for the anharmonic core component in germanium and the intrinsic fact that germanium with its many more electrons is simply more complex computationally.

The experimentally measured structure factors for silicon [including the (222)] are all slightly larger than the calculated values. Roughly speaking, this means that the bond charge in silicon is more sharply peaked than would be inferred from theory. Conversely, in germanium the measured values fall below the calculated scattering amplitudes leading to a bond-charge density that is more diffuse than what is calculated. This conclusion assumes that the anharmonic vibrational component is the dominant term at room temperature in the measured intensity of the germanium forbidden reflections. Certainly the assumption concerning the relative sizes of the two scattering terms (bond versus anharmonic) should be experimentally confirmed by measuring the temperature dependence of these reflections.

Our choice of synchrotron radiation to measure these reflections was based on several properties inherent to the source. These included the high degree of natural vertical collimation, which can be used to increase the signal-to-noise ratio, and the continuous nature of the spectrum which facilitated the location of the extremely weak, forbidden reflection. In addition to these unique properties, we expected a substantial increase in flux over that from a standard x-ray tube. In fact, the net flux from the synchrotron was comparable to the conventional source. However, the other advantages (tunability and intrinsic brightness) more than compensated for the lower-than-expected flux.

At present, the first three $(4n \pm 2)$-type forbidden reflections in silicon and germanium have been measured, the two higher-order reflections in both materials having been measured in this work using synchrotron radiation. In the next few years new synchrotron radiation sources will be coming on line with calculated fluxes approximately 3 orders-of-magnitude larger than that from the synchrotron used in this work. Elimination of the first harmonic ($\frac{1}{2}\lambda$) through the use of a double crystal monochromator[29] should allow for a much easier analysis and will permit even higher-order forbidden reflections to be measured. One should, however, first examine what can be gained from these studies.

In silicon at room temperature the anharmonic term has already become comparable in size to

the valence term at the (622) reflection and probably dominates all the germanium forbidden reflections above (222). If information about the valence charge density is to be extracted from these higher-order reflections, the anharmonic contributions must be more accurately determined.

One should perhaps look at the situation in the opposite sense. Using higher-order reflections, it should be possible to study the anharmonic term with only minor interference from the valence term. For example, if we assume the valence term for (666) decreases by a factor of 2 compared to the (622) and the anharmonic term has increased by a factor of 5 (at room temperature), the ratio of anharmonic to valence components would be almost 10:1. In germanium the effect should be even more pronounced.

Studying the integrated intensity of higher-order forbidden reflections versus temperature would provide information on the temperature dependence of the anharmonic term, since this will grow and become dominant at elevated temperatures. The study of a variety of these higher-order reflections would allow one to check the theoretically predicted dependence of the anharmonic term on the product of the Miller indices. [A similar study has been made with neutrons. However, due to the large experimental uncertainties, the validity of the (*hkl*) scaling could not be positively confirmed.] Going to high-order reflections requires the use of shorter wavelengths, and the problem of multiple reflections becomes more severe. The sharpening of the peaks and wavelength selectability associated with synchrotron radiation may be a way to circumvent this difficulty.

Nonetheless, still to be answered are two other important questions concerning temperature effects on the valence charge density: (1) Is the valence charge distribution in the diamond structure temperature dependent? (2) Is the vibrational amplitude of the valence electrons different from that of the core? An accurate determination of the temperature dependence of the lower-order forbidden reflections using synchrotron radiation should be able to answer these questions.

ACKNOWLEDGMENTS

The authors would like to thank Professor B. McDaniel and the entire staff at the Wilson Synchrotron for their cooperation. This work was supported by a grant (DMR7826662) from the National Science Foundation and from the Materials Science Center at Cornell University (DMR7681083).

[1]W. H. Bragg, Proc. R. Soc. London 33, 304 (1921).
[2]B. Dawson, Proc. R. Soc. London A 298, 264 (1967).
[3]R. J. Weiss and R. Middleton (private communication to B. Dawson from authors. See Ref. 2).
[4]M. Renninger, Acta Crystallogr. 8, 606 (1955).
[5]R. Colella and A. Merlini, Phys. Status Solidi 18, 157 (1966).
[6]J. J. De Marco and R. J. Weiss, Phys. Rev. 127, 690 (1962).
[7]M. Fehlman and I. Fujimoto, J. Phys. Soc. Jpn. 38, 208 (1975).
[8]I. Fujimoto, Phys. Rev. B 9, 591 (1974).
[9]S. Göttlicher and W. Wölfel, Z. Elektrochem. 63, 891 (1959).
[10]L. D. Jennings, J. Appl. Phys. 40, 5038 (1969).
[11]M. Renninger, Z. Kristallogr. 113, 99 (1960).
[12]J. B. Roberto and B. W. Batterman, Phys. Rev. B 9, 3220 (1970).
[13]R. J. Weiss (private communication to B. Dawson from author. See Ref. 22).
[14]J. B. Roberto, B. W. Batterman, and D. T. Keating, Phys. Rev. B 9, 2590 (1974).
[15]D. H. Bilderback and R. Colella, Phys. Rev. B 11, 793 (1975).
[16]P. Trucano and B. W. Batterman, Phys. Rev. B 6, 3659 (1972).
[17]B. Dawson and B. T. M. Willis, Proc. R. Soc. London A 298, 307 (1967).
[18]D. T. Keating, A. G. Nunes, B. W. Batterman, and J. B. Hastings, Phys. Rev. B 4, 2472 (1971).
[19]J. B. Roberto, B. W. Batterman, and D. T. Keating, Phys. Status Solidi B 59, K59 (1973).
[20]J. B. Hastings and B. W. Batterman, Phys. Rev. B 12, 5580 (1975).
[21]P. F. Price, E. N. Maslen, and S. L. Mair, Acta Crystallogr. A 34, 183 (1978).
[22]B. Dawson, Proc. R. Soc. London A 298, 395 (1967).
[23]Syton is a tradename for a colloidal suspension polish manufactured by Monsanto.
[24]D. M. Mills, Ph.D. thesis, Cornell University, MSC #4120, 1979 (unpublished).
[25]J. B. Roberto, B. W. Batterman, and D. T. Keating, Phys. Rev. B 9, 2590 (1974).
[26]G. F. Bacon, Acta Crystallogr. A 28, 357 (1972).
[27]B. Dawson, Proc. R. Soc. London A 298, 379 (1967).
[28]P. J. E. Aldred and M. Hart, Proc. R. Soc. London A 332, 223 (1973).
[29]A channel-cut monochromator with a "weak link" for harmonic rejection has been built by the authors and tested at CHESS, the Cornell High Energy Synchrotron Source. With the storage ring running at 5 GeV and 3 mA (well below its optimum design capacities) an increase in flux of more than 2 orders of magnitude over that has already been attained in this work.

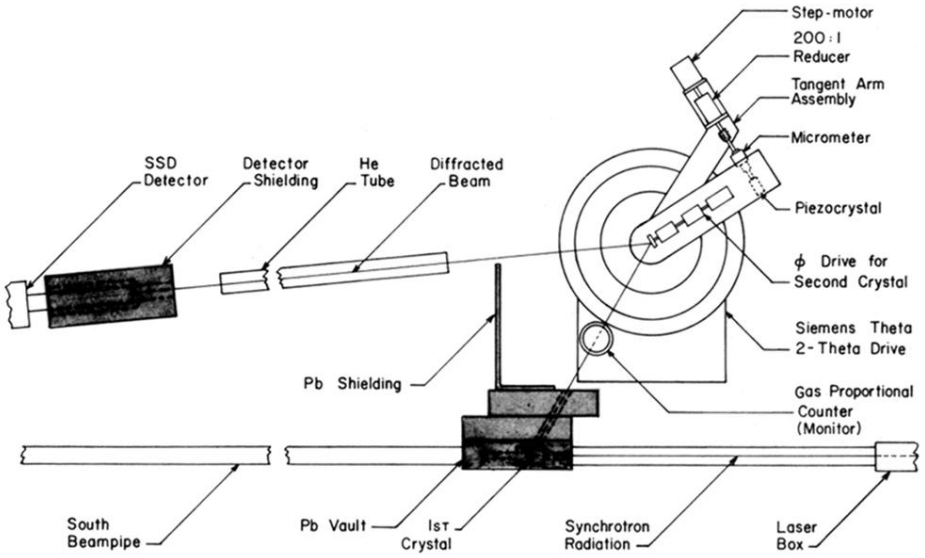

FIG. 2. Schematic diagram of experimental setup used to measure the forbidden reflections.